

A Nanoscale Mechanism of Fatigue in Ionic Solids

Emily A. A. Jarvis

National Institute of Standards and Technology, 100 Bureau Drive, Stop 8380,
Gaithersburg, Maryland 20899-8380

Emily A. Carter*

Department of Mechanical and Aerospace Engineering and Program in Applied and
Computational Mathematics, Princeton University, Princeton, New Jersey 08544-5263

Received December 29, 2005; Revised Manuscript Received February 1, 2006

ABSTRACT

We employ periodic density functional theory to explore the effect of cyclic tensile loading on the behavior of alumina in the threshold region of crack formation. We find evidence for nanoscale fatigue when the alumina lattice is subjected to uniaxial tensile loading and unloading and tensile stresses normal to the applied load. It is possible that such atomic-scale fatigue impacts the durability of ceramics, since the highly ionic bonding requires near-ideal lattice structures in order to maintain cohesive strength.

Advanced design and applications of materials require specification of the ideal material properties as well as an appreciation for how these properties are modified through physical and chemical degradation. In particular, as the pursuit of novel properties associated with nanodevices drives length scales ever smaller, an atomic-level understanding of materials properties becomes essential. Interestingly, some properties that have been well-characterized for decades at the macroscopic level become much more elusive at the microscopic level. The competing mechanisms associated with materials failure make it particularly challenging to characterize over a variety of length scales.

The cause and impact of fatigue processes in materials have been of interest to engineers and materials scientists for decades. The impact of fatigue properties in ceramics is critical in a variety of advanced structural applications. Fracture and fatigue behavior of alumina, Al_2O_3 , have been investigated as they relate to a variety of pertinent properties and conditions such as impact strength,¹ temperature dependence,^{2,3} static and cyclic loading,^{4–9} grain size,^{7,10} crack closure,¹¹ and formation of dislocations and twinning due to abrasion.¹² Similar fracture properties have been explored for oxide scales,¹³ aluminum/alumina interfaces,¹⁴ and other ceramics such as silicon carbide,¹⁵ silicon nitride,^{16,17} and partially stabilized zirconia.¹⁸ Recently, studies of glass fracture via atomic force microscopy have shown similarities between ductile and brittle fracture, with the primary difference being order of magnitude length scale differences rather than fundamental mechanisms of failure,¹⁹ potentially

opening a wealth of understanding from the extensive literature of fatigue in metals for application to brittle ceramics. Although significant contributions have been made in terms of analytical modeling of fatigue and fracture as well as some atomistic and ab initio dynamics, such as those detailed in refs 20–34, a detailed atomic-level understanding of the many competing factors in such materials failure remains far from complete.

Previously, we discussed the effects of oxidation on atomic-level mechanisms of crack formation in aluminum.³⁵ We showed how local changes to the electron density arising from aluminum oxidation hold significant implications for materials properties. Namely, the highly localized electron density of the large band gap oxide Al_2O_3 leads to nanocrack formation at considerably smaller tensile strains than required for irreversible crack formation in aluminum. Furthermore, the ionic bonding in Al_2O_3 results in significant relaxations of the surface upon crack formation, potentially inhibiting healing of small cracks. This feature, whereby alumina experiences dramatic surface relaxations due to the ionic nature of its bonding, is critical to our present discussion.

Here we show that the ionic bonding of the alumina crystal may lead to atomic-scale fatigue-type processes. Using periodic density functional theory (DFT)³⁶ within the generalized gradient approximation (GGA) (PW91)³⁷ for the electron exchange and correlation potential as implemented in the Vienna Ab Initio Simulation Package (VASP),³⁸ we investigate the “threshold” region of crack formation in $\alpha\text{-Al}_2\text{O}_3$, i.e., where introduced nanocrack defects are small enough that it is energetically favorable for a crystal with

* To whom correspondence may be addressed. E-mail: eac@princeton.edu.

an equilibrium bulk structure to heal the void rather than create two surfaces. Crack formation perpendicular to the **c**-axis of the α - Al_2O_3 hexagonal cell was investigated for three distinct cases: (1) with in-plane (**a** and **b**) lattice vectors fixed to ideal bulk values, (2) with compression of these lattice vectors by $\approx 5\%$, and (3) with expansion of these lattice vectors by $\approx 5\%$, corresponding to a local change of 0.1 \AA in Al–O bond lengths. These local bonding defects, introduced through compression or expansion of the periodic cell, are designed to approximate a locally strained region at a crack tip rather than global crystal strain.

Our calculations employed the standard VASP ultrasoft pseudopotentials (VASP, version 4.4.4) to replace the core electrons plus nuclei; a nonlinear core correction to the exchange-correlation functional was included for Al. We tested total energy convergence with respect to **k**-point sampling density and kinetic energy cutoff of the plane wave basis for bulk α - Al_2O_3 . As a result, we employed a **k**-point sampling of $3 \times 3 \times 1$ for the hexagonal unit cell of Al_2O_3 , kinetic energy cutoffs of 338 eV for the planewave basis, and 554 eV for the augmentation charge basis needed for the ultrasoft pseudopotentials. The chosen cutoffs and **k**-point density resulted in total energies converged to within the meV/atom range.

We optimized the volume of the primitive crystals by performing a series of single point energy calculations uniformly scaling the lattice vectors within $\approx 5\%$ of the equilibrium value and fitting to the Murnaghan equation of state.³⁹ For the ideal bulk crystal cases, the optimized cell lattice vectors (which are within $\approx 1\%$ of experiment⁴⁰) were used in the construction of the cells used in the crack simulation, with a vacuum region introduced as a localized planar defect to increase the periodic cell lattice vector in the direction perpendicular to the Al_2O_3 (0001) planes, to introduce a crack parallel to the basal plane in the periodic cell. The compressed and expanded periodic cells were similar to the ideal bulk crystal periodic cells except that the in-plane lattice vectors were compressed or expanded by $\approx 5\%$, respectively. Test cases with slab thicknesses of 6, 12, and 18 Al_2O_3 units were investigated. From these calculations, we determined that 6 Al_2O_3 units (≈ 18 atomic “layers”) for Al_2O_3 were sufficient to obtain results converged with respect to slab thickness, i.e., to achieve results representative of a bulk crystal rather than a thin film.

Figure 1 displays the bulk hexagonal α - Al_2O_3 unit cell and a location between adjacent Al planes parallel to (0001) where nanocracks are introduced. The direction of crack formation was chosen because alumina has been shown to grow with surfaces parallel to the (0001) planes⁴¹ upon aluminum oxidation, and the particular crack surface termination chosen is the most stable low-index surface of alumina.^{42–44} Cases where lattice strain is introduced through compression or expansion in the direction of crack propagation are more indicative of a realistic scenario of materials failure since the ideal crystalline lattice will be strained at a crack front.

To simulate crack formation, we introduce tensile strain in the form of nanocracks parallel to the bulk (0001) planes

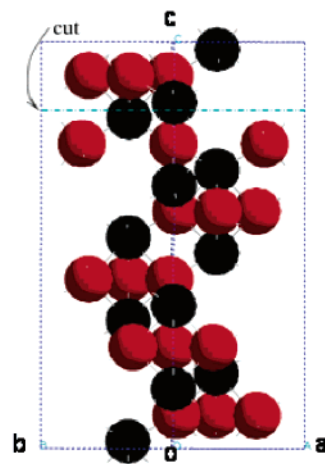


Figure 1. Bulk hexagonal cell of α - Al_2O_3 with aluminum represented by black spheres and oxygen by red spheres. The dashed line indicates the location between adjacent Al planes parallel to (0001) where nanocracks are introduced.

for α - Al_2O_3 and allow the ionic coordinates to relax so as to minimize the energy using a conjugate gradient relaxation from the initial bulk ionic coordinates. We introduce successively wider nanocracks until the relaxed coordinates can no longer heal the crack, as evidenced by a lack of sufficient electron density percolating across the two surfaces.³⁵ We then investigate possible fatigue-type processes due to cyclic (tensile) loading and unloading in this threshold region of crack formation. Surfaces with relaxed ionic coordinates are brought back together to mimic unloading of a sample, i.e., the nanocrack thickness is decreased, to replicate the values of strain at which the defect site would have healed when starting from bulk ionic coordinates.

Typically, fatigue is evidenced through stress–strain hysteresis loops, which illustrate the irreversibility of the fatigue process. In that case, a stress (force per unit area) is plotted versus a dimensionless strain arising from a change in length, and the irreversible energy dissipation is given by the enclosed area of the loop.⁴⁵ For our first principles investigation of fatigue at the atomic level, we searched for hysteresis in plots of energy versus increase in **c** lattice vector resulting from introduction of a nanocrack at a site between adjacent Al planes. These plots relate similar phenomena. The energy increases, relative to the equilibrium lattice structure, with increasing nanocrack width parallel to the (0001) planes until the energy of creating two surfaces is less than or equal to the energetic cost of healing the introduced crack. The amount by which the energy is increased is directly related to the load applied and to the size of defect introduced, while the introduction of increasing vacuum region along the **c** lattice vector (the incipient crack) can be represented as an increasing strain relative to the ideal bulk lattice, as long as it is energetically favorable for the crystal to heal the nanocrack rather than form two isolated surfaces. Any energy – **c**-vector hysteresis loop we observe would represent irreversibility in the pathways taken by the atoms during cyclic tensile loading.

For the cases where the in-plane lattice vectors were either fixed to bulk values or compressed, no hysteresis in total

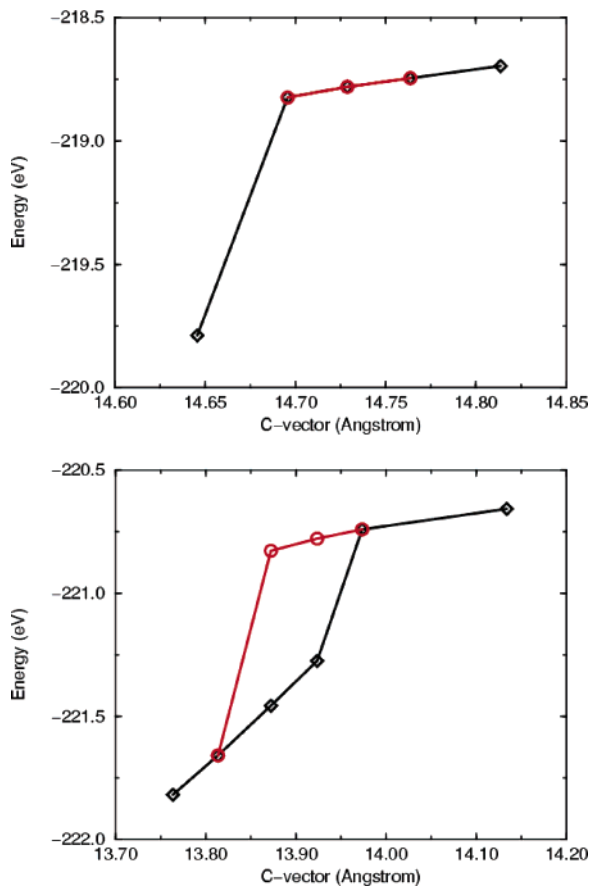


Figure 2. (a) Energy versus *c* lattice vector curve for the case with **a** and **b** lattice vectors compressed by 5%. The black diamonds indicate the points along the curve where the ions at the nanocrack start with perfect bulk crystal ionic coordinates and the red circles indicate points where ionic relaxation started with relaxed surface coordinates at the nanocrack. No hysteresis is observed; the final relaxed structures are identical for all points whether starting from perfect bulk or relaxed surface ionic coordinates at the nanocrack. (b) Energy versus *c* lattice vector curve for the case with **a** and **b** lattice vectors expanded by 5%. The black diamonds indicate the points along the curve where the ions at the nanocrack start with perfect bulk ionic coordinates and the red circles indicate points where ionic relaxation started with relaxed surface coordinates at the nanocrack. In this case, hysteresis is observed; the final relaxed structures differ for several points depending on whether the starting conditions included perfect bulk (loading) or relaxed surface coordinates at the nanocrack (unloading).

energy versus crack surface separation was observed. In these cases, the relaxed ionic coordinates were the same regardless of whether the nanocrack surface regions initially were terminated by bulk lattice positions or relaxed surface coordinates. Figure 2a displays the energy versus *c* lattice vector curve for the case with **a** and **b** lattice vectors compressed by 5%. The cyclic loading pathway is completely reversible, with no energy dissipation predicted.

With the in-plane lattice either fixed to a perfect bulk crystal or compressed, considerable relaxation of the surface ions occurs with crack formation. The dramatic extent of these relaxations (greater than 80% inward relaxation for the aluminum layer that terminates the crack surfaces) has its origin in the highly ionic nature of the Al–O bond in alumina. Exposing a bare, nominally Al³⁺ ion on a surface

is very unfavorable electrostatically; hence, the surface Al layer relaxes almost completely into the $\approx O^{2-}$ plane beneath it. Similar surface relaxations with in-plane lattice vectors fixed to bulk α -Al₂O₃ have been discussed previously.^{46,47} Most of the surface relaxation effect is confined to vertical relaxation, with some limited in-plane rearrangement. These vertical relaxations are reversed readily as soon as the surfaces are brought into closer proximity to one another. In other words, there is little or no effective barrier to healing such nanocracks regardless of the detailed local surface structure within this threshold region of crack formation.

Contrary to the cases with the ideal or compressed lattice, a clear hysteresis is apparent when the lattice is subject to in-plane expansion. This is shown in Figure 2b. In this case, the relaxed ionic coordinates in the crystal depend sensitively on the initial coordinates of the ions near the nanocrack region. When a nanocrack defect is introduced between the bulk ionic positions of the adjacent aluminum planes, the crystal heals the defect for the cases along the lower curve of the hysteresis loop. The resulting structure is uniformly strained when healing the local defect. However, when similar nanocrack defects are introduced to a crystal with relaxed surface ionic coordinates at the defect site, a local minimum is accessed upon relaxation. In these cases, the defect remains localized at the original site of the nanocrack instead of uniformly straining the crystal, thereby producing a higher energy structure. Thus, if the initial crack formed upon tensile loading exists long enough for the crack surfaces to adopt their preferred surface structure (with Al³⁺ ions buried in the oxygen ion layer beneath it), it will not heal properly upon unloading. *This may very well occur upon unloading of a crack tip, where strains are likely to be tensile. Thus the “healed” crack may end up with a defective structure that is weakened, ultimately resulting in fatigue.*

Figure 3 presents a qualitative display of the hysteresis shown quantitatively in Figure 2b, by depicting the ionic coordinates adopted during a tensile loading/unloading cycle. The upper section of the loop, accessed during unloading, shows nanocracks persisting after relaxation to a local minimum. These structures correspond to the higher energy curve of the hysteresis loop. The lower section of the loop, accessed during loading, initially contained ideal ionic coordinates for the expanded lattice for all ions on either side of the nanocrack. This lower section of the loop exhibits relaxed structures where the nanocrack heals. Although the surface relaxations of the expanded in-plane lattice are broadly similar to those with a compressed or ideal lattice, the moderate expansion of the lattice perpendicular to crack formation permits even greater relaxation to shield the “bare” surface ions. These surface stabilization effects are not as readily reversed upon decreasing nanocrack thickness, hence a local minimum is accessed upon relaxation of these surface structures. Accordingly, a nanoscale stress–strain hysteresis corresponding to atomic-level fatigue is observed.

The highly ionic bonding in alumina and other metal oxides bears significant implications for nanoscale mechanisms of materials failure. The electron density of the ionic, brittle alumina is highly localized relative to aluminum metal,

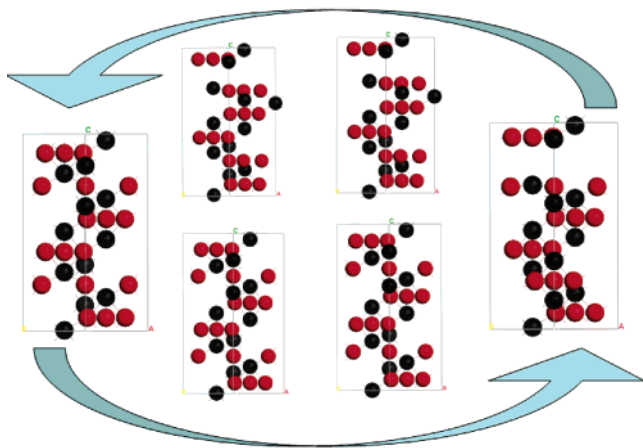


Figure 3. Hexagonal cells of $\alpha\text{-Al}_2\text{O}_3$ with optimized ionic coordinates for the nanocrack points comprising the hysteresis loop of Figure 2b. The upper section of the loop shows nanocracks persisting after optimization to a local minimum. These structures correspond to the higher energy curve of the hysteresis loop. The lower section of the loop corresponds to structures relaxed from perfect bulk ionic coordinates for the expanded lattice, where the nanocrack heals. The arrows indicate the fatigue cycle where the left side and lower portion represent “pulling” on the ideal expanded crystal during loading and the right side and upper portion display the nanocrack being “pushed” back together after unloading.

resulting in crack formation with much smaller tensile loads.³⁵ Additionally, this ionic bonding may lead to large local relaxations at a defect site, resulting in irreversible crack formation at nanocracks which otherwise would not represent a failure defect in the crystal. This atomic-level mechanism of materials failure may contribute to fatigue crack growth. Similar mechanisms, whereby locally strained ionic bonding leads to large relaxations at defect sites, could be at work in the degradation of grain (boundary) bridging more commonly associated with fatigue in certain ceramics, including alumina.⁴⁸ While our idealized parallel plane structure for a crack is of course only a crude approximation to a crack tip, we expect the qualitative trends to hold for an actual tip with nonparallel crack surfaces (the aperiodic nature of such a real crack makes it impossible to simulate with first principles quantum mechanics at this point). Although the results shown here apply specifically to $\alpha\text{-Al}_2\text{O}_3$, it is anticipated that similar atomic-scale fatigue mechanisms would influence a variety of other ionic solids and films. Such atomic-scale fatigue may impact the durability of ceramics and semiconductors⁴⁹ in general, since the localized bonding in both materials families requires very specific lattice structures in order to maintain cohesive strength. Lastly, although the effects of water are not considered here, the dramatic impact of water adsorption on oxide surface energies^{44,50} indicates it could play a crucial role in modifying local bonding at defect sites where crack propagation occurs. Providing an atomic-scale understanding of how such local changes in the oxide bonding modify the macroscopic materials properties represents an area of ongoing research.

Acknowledgment. We are grateful to the Air Force Office of Scientific Research for funding this research.

References

- (1) Sarkar, B. K.; Glinn, T. G. *J. Mater. Sci.* **1969**, *4*, 951–954.
- (2) Sarkar, B. K.; Glinn, T. G. *J. Philos. Mag.* **1969**, *20*, 1285–1287.
- (3) Wiederhorn, S. M.; Hockey, B. J.; Roberts, D. E. *Philos. Mag.* **1973**, *28*, 783–796.
- (4) Ewart, L.; Suresh, S. *J. Mater. Sci. Lett.* **1986**, *5*, 774–778.
- (5) Ewart, L.; Suresh, S. *J. Mater. Sci.* **1987**, *22*, 1173–1192.
- (6) Gilbert, C. J.; Dauskardt, R. H.; Ritchie, R. O. *Ceram. Int.* **1997**, *23*, 413–418.
- (7) Gilbert, C. J.; Petrány, R. N.; Ritchie, R. O.; Dauskardt, R. H.; Steinbrech, R. W. *J. Mater. Sci.* **1995**, *30*, 643–654.
- (8) Li, M.; Guiu, F. *Scr. Metall. Mater.* **1995**, *32*, 1549–1552.
- (9) Guiu, F. *J. Mater. Sci. Lett.* **1978**, *13*, 1357–1361.
- (10) Llorca, J.; Steinbrech, R. W. *J. Mater. Sci.* **1991**, *26*, 6383–6390.
- (11) Gilbert, C. J.; Ritchie, R. O. *Fatigue Fract. Eng. Mater. Struct.* **1997**, *20*, 1453–1466.
- (12) Inkson, B. J. *Acta Mater.* **2000**, *48*, 1883–1895.
- (13) Hancock, P.; Nicholls, J. R. *Mater. Sci. Technol.* **1998**, *4*, 398–406.
- (14) McNaney, J. M.; Cannon, R. M.; Ritchie, R. O. *Acta Mater.* **1996**, *44*, 4713–4728.
- (15) Gilbert, C. J.; Ritchie, R. O. *Acta Mater.* **1998**, *46*, 609–616.
- (16) Gilbert, C. J.; Ritchie, R. O. *Eng. Fract. Mech.* **1998**, *60*, 303–313.
- (17) Tsuruta, K.; Nakano, A.; Kalia, R. K.; Vashisha, P. *J. Am. Ceram. Soc.* **1998**, *81*, 433–436.
- (18) Hoffman, M. J.; Mai, Y.-W.; Dauskardt, R. H.; Ager, J.; Ritchie, R. O. *J. Mater. Sci.* **1995**, *30*, 3291–3299.
- (19) Célarié, F.; Prades, S.; Bonamy, D.; Ferrero, L.; Bouchaud, E.; Guillot, C.; Marlière, C. *Phys. Rev. Lett.* **2003**, *90*, 75, 504. Célarié, F.; Prades, S.; Bonamy, D.; Dickele, A.; Bouchaud, E.; Guillot, C.; Marlière, C. *App. Surf. Sci.* **2003**, *212*, 92–96. Marlière, C.; Prades, S.; Célarié, F.; Dalmas, D.; Bonamy, D.; Guillot, C.; Bouchaud, E. *J. Phys.: Condens. Matter* **2003**, *15*, S2377–S2386.
- (20) Macha, E.; Sonsino, C. M. *Fatigue Fract. Eng. Mater. Struct.* **1999**, *22*, 1053–1070.
- (21) Hasselman, D. P. H.; Coppola, J. A.; Krohn, D. A.; Bradt, R. C. *Mater. Res. Bull.* **1972**, *7*, 769–772.
- (22) Elber, W. *Eng. Fract. Mech.* **1970**, *2*, 37–45.
- (23) Thomson, R.; Carlsson, A. E. *Philos. Mag. A* **1997**, *75*, 749–769.
- (24) Gerde, E.; Marder, M. *Nature* **2001**, *413*, 285–288.
- (25) Vasudeven, A. K.; Sadananda, K.; Louat, N. *Mater. Sci. Eng., A* **1994**, *A188*, 1–22.
- (26) McNaney, J. M.; Gilbert, C. J.; Ritchie, R. O. *Acta Mater.* **1999**, *47*, 2809–2819.
- (27) Schiøtz, J.; Carlsson, A. E.; Canel, L. M.; Thomson, R. *Mater. Res. Soc. Symp. Proc.* **1996**, *408*, 237–248.
- (28) Schiøtz, J.; Canel, L. M.; Carlsson, A. E. *Phys. Rev. B* **1997**, *55*, 6211–6221.
- (29) Rice, J. R.; Hawk, D. E.; Asaro, R. J. *Int. J. Fract.* **1990**, *42*, 301–321.
- (30) Sastry, V.; Farkas, D. *Mater. Res. Soc. Symp. Proc.* **1996**, *408*, 217–228.
- (31) Thomson, R.; Carlsson, A. E. *Mater. Res. Soc. Symp. Proc.* **1996**, *408*, 229–235.
- (32) Hayes, R. L.; Ortiz, M.; Carter, E. A. *Phys. Rev. B* **2004**, *69*, 172104.
- (33) Abraham, F. F.; Brodbeck, D.; Rudge, W. E.; Broughton, J. Q.; Schneider, D.; Land, B.; Lifka, D.; Gerner, J.; Rosenkrantz, M.; Skovvira, J. *Model. Simul. Mater. Sci. Eng.* **1998**, *6*, 639–670.
- (34) Van der Ven, A.; Ceder, G. *Acta Mater.* **2004**, *52*, 1223–1235.
- (35) Jarvis, E. A. A.; Hayes, R. L.; Carter, E. A. *ChemPhysChem* **2001**, *2*, 55–59.
- (36) Hohenberg, P.; Kohn, W. *Phys. Rev.* **1964**, *136*, B864–B871. Kohn, W.; Sham, L. J. *Phys. Rev.* **1965**, *140*, A1133–A1138.
- (37) Perdew, J. P. In *Electronic Structure of Solids*; Ziesche, P., Eschrig, H., Eds.; Akademie Verlag: Berlin, 1991; p 11. Perdew, J. P.; Chevary, J. A.; Vosko, S. H.; Jackson, K. A.; Pederson, M. R.; Singh, D. J.; Fiolhais, C. *Phys. Rev. B* **1992**, *46*, 6671–6687. Perdew, J. P. *Phys. Rev. B* **1986**, *33*, 8822–8824; *34*, 7406 (E). Perdew, J. P.; Wang, Y. *Phys. Rev. B* **1992**, *45*, 13244–13249.
- (38) Certain commercial equipment and software are identified in this paper in order to specify the experimental procedure adequately. Such identification is not intended to imply recommendation or endorsement by the National Institute of Standards and Technology, nor is it intended to imply that the software or equipment identified are necessarily the best available for the purpose. Kresse, G.; Hafner, J. *Phys. Rev. B* **1993**, *47*, 558–561. Kresse, G.; Furthmüller, J. *Comput. Mater. Sci.* **1996**, *6*, 15–50.

- (39) Murnaghan, F. D. *Proc. Natl. Acad. Sci.* **1944**, *30*, 2344.
- (40) d'Amour, H.; Schiferl, D.; Denner, W.; Schultz, H.; Holzapfel, W. B. *J. Appl. Phys.* **1978**, *49*, 4411–4416.
- (41) Clausen, E. M., Jr.; Hren, J. J. *Mater. Res. Soc. Symp. Proc.* **1985**, *41*, 381–386.
- (42) Mackrodt, W. C.; Davey, R. J.; Black, S. N.; Docherty, R. J. *Cryst. Growth* **1987**, *80*, 441–446.
- (43) Manassidis, I.; De Vita, A.; Gillan, M. J. *Surf. Sci.* **1993**, *285*, L517–L521. Manassidis, I.; Gillan, M. J. *J. Am. Ceram. Soc.* **1994**, *77*, 335–338.
- (44) Wang, X.-G.; Chaka, A.; Scheffler, M. *Phys. Rev. Lett.* **2000**, *84*, 3650–3653.
- (45) See for example: Erber, T. *Eur. J. Phys.* **2001**, *22*, 491–499.
- (46) Verdozzi, C.; Jennison, D. R.; Schultz, P. A.; Sears, M. P. *Phys. Rev. Lett.* **1999**, *82*, 799–802.
- (47) Jarvis, E. A. A.; Christensen, A.; Carter, E. A. *Surf. Sci.* **2001**, *487*, 55–76.
- (48) See for example: Lathabai, S.; Rodel, J.; Lawn, B. R. *J. Am. Ceram. Soc.* **1991**, *74*, 1340–1348. Li, M.; Guiu, F. *Acta Metal. Mater.* **1995**, *43*, 1871–1884. Kruzic, J. J.; Cannon, R. M.; Ritchie, R. O. *J. Am. Ceram. Soc.* **2004**, *87*, 93–103. Attaoui, H.; Saâdaoui, M.; Chevalier, J.; Gilbert, F. *J. Am. Ceram. Soc.* **2005**, *88*, 172–178.
- (49) Hayes, R. L.; Carter, E. A. *J. Chem. Phys.* **2005**, *123*, 244704.
- (50) Chevalier, J.; et al. *Nano Lett.* **2005**, *5*, 1297–1301.

NL0525655